

Analysis of bulk void regions

Sebastian Bustamante ¹ Jaime E. Forero-Romero²

¹*Instituto de Física - FCEN, Universidad de Antioquia, Calle 67 No. 53-108, Medellín, Colombia*

²*Departamento de Física, Universidad de los Andes, Cra. 1 No. 18A-10, Edificio Ip, Bogotá, Colombia*

2 May 2014

ABSTRACT

Key words: Cosmology: large-scale Structure of Universe, galaxies: star formation - line: formation

1 INTRODUCTION

The spatial distribution of galaxies describes a web-like pattern, the so-called cosmic web. Today it is understood that such configuration is driven by gravitational instabilities. ...

Relevant information about previous works and current state of the art.

2 THE SIMULATION

As it was previously mentioned, we use an unconstrained cosmological simulation, the Bolshoi simulation, to identify the possible large scale environment of the Local Group. This is a similar approach to the one already used by [reference here].

The Bolshoi simulation follows the non-linear evolution of a dark matter density field on a cubic volume of size $250h^{-1}\text{Mpc}$ sampled with 2048^3 particles. The cosmological parameters in the simulation are $\Omega_m = 0.27$, $\Omega_\Lambda = 0.73$, $h = 0.70$, $n = 0.95$ and $\sigma_8 = 0.82$ for the matter density, cosmological constant, dimensionless Hubble parameter, spectral index of primordial density perturbations and normalization for the power spectrum. The mass of each particle in the simulation is $m_p = 1.4 \times 10^8 h^{-1} M_\odot$. We identify halos with two algorithms, the Friends-of-Friends [reference here] algorithm and the Bound Density Maximum algorithm.

3 ALGORITHMS TO QUANTIFY THE COSMIC WEB

3.1 The tidal web (T-web)

The first algorithm we use to identify the cosmic web is based upon the diagonalization of the tidal tensor, defined as the Hessian of a normalized gravitational potential

$$T_{\alpha\beta} = \frac{\partial^2 \phi}{\partial x_\alpha \partial x_\beta} \quad (1)$$

where the physical gravitational potential has been rescaled by a factor $4\pi G \bar{\rho}$ in such a way that ϕ satisfies the following equation

$$\nabla^2 \phi = \delta, \quad (2)$$

where $\bar{\rho}$ is the average density in the Universe, G is the gravitational constant and δ is the dimensionless matter overdensity.

3.2 The velocity web (V-web)

We also use a kinematical method to define the cosmic-web environment in the simulation. The method has been thoroughly described in XXX and applied to study the shape and spin alignment in the Bolshoi simulation here XX. We refer the reader to these papers to find a detailed description of the algorithm, its limitations and capabilities. Here we summarize the most relevant points for the discussion.

The V-web method for environment finding is based on the local shear tensor calculated from the smoothed DM velocity field in the simulation. The central quantity is the following dimensionless quantity

$$\Sigma_{\alpha\beta} = -\frac{1}{2H_0} \left(\frac{\partial v_\alpha}{\partial x_\beta} + \frac{\partial v_\beta}{\partial x_\alpha} \right) \quad (3)$$

where v_α and x_α represent the α component of the comoving velocity and position, respectively. $\Sigma_{\alpha\beta}$ can be represented by a 3×3 symmetric matrix with real values, that ensures that is possible to diagonalize and obtain three real eigenvalues $\lambda_1 > \lambda_2 > \lambda_3$ whose sum (the trace of $\Sigma_{\alpha\beta}$) is proportional to the divergence of the local velocity field smoothed on the physical scale \mathcal{R} .

The relative strength of the three eigenvalues with respect to a threshold value λ_{th} allows for the local classifica-

* sbustama@pegasus.udea.edu.co

tion of the matter distribution into four web types: voids, sheets, filaments and peaks, which correspond to regions with 3, 2, 1 or 0 eigenvalues with values larger than λ_{th} . Below we shall discuss a novel approach to define an adequate threshold value based on the visual impression of void regions, furthermore we study other possible values based on other visual features of the cosmic web.

3.3 The cosmic web in Bolshoi

Both established schemes to quantify the cosmic web depend on continuous and smooth physical quantities, i.e the peculiar velocity field and the density field. To calculate these quantities, a discretization over the volume of the simulation is performed, so all the properties are reduced to single values associated to discrete cells. According to this, we divide the overall volume into $(256)^3$ cells, so each cell has an associated comoving cubic volume of 0.98 Mpc h^{-1} . Finally, in order to reduce possible effects due to the discretization process, a gaussian softening is performed between neighbour cells.

Once defined the numerical details about both classification schemes, we shall analyse the dependence on the threshold value λ_{th} for each one. For this, we shall use the distribution of dark matter halos as tracer of the underlying matter field in order to be more consistent with available observational data. In the figure 1 we calculate fractions of halos within each one of the defined environments based upon the FOF catalogue of the simulation and for an extensive λ_{th} range. Then we look for some key feature that could indicated us a possible optimal value of the λ_{th} value. One first step forward our quest is the behaviour of the V-web scheme compared with the T-web. As was previously established by **Hoffman et al. (2012)** and as can be seen in the figure 1, V-web scheme is significantly more sensible to variations of the λ_{th} value, since all fractions of halos for the V-web change significantly in the range $[0, 0.4]$, whereas, for the T-web scheme, fractions change smoothly throughout all λ_{th} range covered. From this, it is then expected that the optimal λ_{th} value for the V-web scheme is less than the T-web value.

The more notorious characteristic of the figure 1 is the behaviour of the fraction of halos within sheet regions for both web schemes, increasing until a local maximum, and then decreasing. The increasing or decreasing rate of the fraction of halos for some region could be interpreted as a measure of the degree of non-linearity of such region for some specific λ_{th} value. For example, filaments and knots, that are the most non-linear regions of the universe, have a negative rate for all covered λ_{th} range. In the case of voids, the situation is completely opposite, where fractions of halos increase in everywhere. If we think in terms of the underlying matter field of the cosmic web, λ_{th} is just a cutting parameter between highly non-linear regions (filament and knots) and low non-linear (voids and sheets). Furthermore, if we take into account that dark matter halos are much more likely to form in highly non-linear regions, it is expected the obtained behaviour of the fractions of halos for voids, filaments and knots as we increase the λ_{th} value. However, the behaviour of the fraction of halos in sheets is less clear, increasing for low λ_{th} values (such as voids) and decreasing for higher λ_{th} values (such as filaments and knots). This indi-

cates the transitional character of sheet regions in the cosmic web. Our proposal here is to select as optimal λ_{th} the value where the fraction of sheets reaches a local maximum. According to this, we find for the T-web scheme an optimal value $\lambda_{opt}^T = 0.36$ and for the V-web scheme $\lambda_{opt}^V = 0.20$. In the figure 2 we show the visual impression of the cosmic web along with the density field for different λ_{th} values including the optimal values. It can be noticed that the found optimal values reproduce well the visual impression.

As we have taken halos as tracers of the cosmic web, we analyse distributions of mass and peculiar velocity in order to assign typical values to each type of environment. In the figure 3 we calculate both distributions for both web schemes and using the FOF catalogue of the simulation. Thick lines correspond to the median of the distribution and filled regions limited by dashed lines correspond to quartiles Q_1 and Q_3 , it means, 50% of all halos are within such regions for every λ_{th} value and for each type of environment. We rather use median and quartiles as measure of dispersion because there are some very unusual and extreme values that makes the usual analysis based upon means and standard deviations less reliable.

A first interesting feature of the figure 3 is the median mass for each region. In the case of the T-web, although dispersions of the distribution of mass for each environment are considerably overlapped each other, the median value is very well-differentiated among types of environment, indicating that it is possible to assign typical values of mass to each region, and being consistent with expectations, where low mass halos are typical in voids until high mass halos in knots. For the case of the V-web scheme, all medians and dispersions are completely overlapped, specially for values grater than the optimal λ_{th} value, indicating that it is not possible to assign typical mass ranges to each environment as quantified by this scheme. For peculiar velocities, this situation is opposite, where V-web scheme is much more adequate to assign typical distributions of velocity to each environment. Although T-web also makes a differentiation in the distributions of velocity, this is very slight compared with the V-web case. These results can be explained by appealing the physical origin of each web scheme. As T-web is based upon the Hessian matrix of the potential field, it is expected all quantities related to the potential, like density field and distribution of halos mass, are well-differentiated among each region, while the V-web scheme, based upon the shear velocity tensor, all dynamical quantities, as the peculiar velocity field and the distribution of the velocity of halos are also expected to be well-differentiated among regions as quantified by this scheme.

Finally, we also calculate typical distributions of the density and peculiar velocity fields in each type of environment, obtaining completely analogous results. Furthermore, we also use a BDM catalogue of the simulation, obtaining very similar conclusions.

4 FINDING BULK VOIDS

4.1 Fractional anisotropy as tracer of voids

According to the recent growing interest in studying galaxy formation in low-density regions as cosmological tests, classi-

fying void regions is becoming an important task in cosmology. Most of those classification schemes for voids in cosmological simulations are based upon the density field, setting a cut off value below which some region becomes a void [references]. Some more advanced classification schemes are based on Voronoi tessellations applied over the tracer particles of the simulation in order to compute the density field. Then, through a watershed transform, a hierarchy of void regions are found [references, ZOBOV algorithm].

As has been established [references], both schemes presented in the previous section (V-web and T-web) for classifying the cosmic web present many advantages compared with classification schemes based completely upon the density field, e.g. a more robust description of the dynamic a kinematic of the cosmic web, a more reliable quantification of the visual impression, among others. With the aim of exploiting all of these advantages, we propose here a novel approach to classify voids in cosmological simulations based entirely on the web schemes.

The original version of the T-web scheme [reference, Hahn] was not successful at reproducing the visual impression of the cosmic web, however, with the introduction of a threshold parameter [reference, Forero-Romero], this scheme, and even the V-web [reference, Hoffman], improved enormously. As this free parameter controls the visual impression provided by each scheme, phenomena like percolation depends on it as well. Percolation is one of the key features of the structure of void regions, indicating how voids are merged among them, and how they permeate all the cosmic web.

In order to deal with percolation of voids in our classification scheme, we introduce the fractional anisotropy as defined in [reference, Libeskind].

$$FA = \frac{1}{\sqrt{3}} \sqrt{\frac{(\lambda_1 - \lambda_3)^2 + (\lambda_2 - \lambda_3)^2 + (\lambda_1 - \lambda_2)^2}{\lambda_1^2 + \lambda_2^2 + \lambda_3^2}} \quad (4)$$

where the eigenvalues are taken from any of the two web schemes. This index, such as it is defined, allows quantifying the local anisotropy degree of the cosmological environment, where $FA = 0$ corresponds to highly isotropic regions and $FA = 1$ anisotropic ones.

In the figure 4 we calculate the FA field over the simulation for both web schemes. The first interesting feature of this figure is the degeneration presented for knots and central regions of voids, where both of them exhibit low to middle values of the FA, indicating a high isotropy regarding the physical properties quantified by each web scheme, i.e. the density field for the T-web and the peculiar velocity for the V-web. For the T-web, the FA field around knots presents a very narrow distribution, whereas for the V-web the same distribution is more spread. This can be explained appealing to the low dispersion of the density field compared with the peculiar velocity in highly non-linear regions like knots. For more linear regions like voids, the behaviour of the FA field is quite similar between both schemes, what is consistent with the equivalence of the T-web and the V-web in the linear regime [reference, Hoffman].

According to the classification scheme adopted for the cosmological environment, voids are regions where $\lambda_3 \leq \lambda_2 \leq \lambda_1 \leq \lambda_{th}$. This implies that the boundaries of void regions are controlled completely by the λ_1 eigenvalue of

the web scheme and the threshold value. Therefore, as we increase the threshold value λ_{th} , all voids grow up progressively through contours of the λ_3 field until certain critical value where they are so large that the visual impression is no longer reproduced. Our objective here is to find a reliable quantity that allows to trace the geometry of void regions as classified by each web scheme. In the figure 6 we calculate the distributions of the fractional anisotropy index and the density field regarding the λ_1 eigenvalue for both web schemes over all the cells of the simulation. Thick lines correspond to the median of the distributions, whereas coloured regions correspond to the 50% of the sample, delimited by quartiles Q_1 and Q_3 .

The first important conclusion is regarding the distribution of the FA index, where there is an almost perfect correlation with the λ_1 eigenvalue for low values of it. This result can be interpreted as an one-dimensional tomography of void regions, where low λ_1 values are associated to the central regions of voids and they are the more isotropic structures found, with FA values close to 0. As we increase the λ_1 value, corresponding to progressively outer layers of void regions, the FA index increases as well, maintaining a perfect correlation approximately until the optimal threshold value for each scheme. Because of the definition of the fractional anisotropy index, it presents the highest values for filaments and very flat sheets, i.e. $FA \lesssim 1$. Therefore, if we extend the λ_{th} value beyond the optimal threshold, such that the outer regions of voids becomes highly anisotropic, it would imply that voids are invading filaments and sheets, so the optimal threshold is a limit value up to which we can have void regions. For other type of environment such as sheets, filaments and knots, the λ_1 eigenvalue does not control their spatial boundaries, so the correlation with the FA index is no longer valid. The larger dispersion in the distribution indicates that contours of the FA field are no longer corresponding to contours of the λ_1 field. Nevertheless, for high λ_1 values, i.e. $\lambda_1 > 1.0$, the median value of the FA index decreases to lower values, indicating the presence of isotropic knots. All of this allows us to conclude that the distribution of the FA with respect to the λ_1 eigenvalue is not only an one-dimensional tomography of voids, but also a sort of one-dimensional projection of the global structure of the cosmic web, starting in highly isotropic central voids, passing through very anisotropic sheets and filaments, until isotropic knot regions.

For the distribution of the density with respect to the λ_1 eigenvalue, it can be appreciated an analogous behaviour, where central regions of voids present the most under-dense values of the overall cosmic web. For outer layers of voids, the density field grows progressively until sheets and filaments are reached. However, the dispersion in the distributions indicates that the geometry of voids as quantified by both web schemes is not compatible with the density field, i.e. contours of the λ_1 eigenvalue do not coincide with contours of the density field. Then, the density is not a reliable quantity to be used as tracer of voids. Furthermore, another advantage of using the FA index instead of the density is the non-monotonous behaviour of the FA median value, with a local maximum that allows to identify the boundaries of void regions.

4.2 Central regions of voids

5 PROPERTIES OF VOIDS

Once defined the proper scheme to classify bulk voids in the simulation, we proceed to analyse their physical properties, like the inertia values, the density and peculiar velocities profiles as calculated over the grid and profiles of number of halos.

5.1 Shape of voids

Quantifying the shape of voids is gaining importance due to cosmological tests such as the Alcock-Paczynski test [Sutter, et.al (2012)], so we compute here the reduced inertia tensor through the next expression in order to determine shape distributions of bulk voids.

$$\tau_{ij} = \sum_l \frac{x_{l,i}x_{l,j}}{R_l^2} \quad (5)$$

where l is an index associated to each cell of the current region, i and j indexes run over each spatial direction and finally R_l is defined as $R_l^2 = x_{l,1}^2 + x_{l,2}^2 + x_{l,3}^2$. All positions are measured from the respective geometric center of each void.

The eigenvalues of the reduced inertia tensor, i.e. the principal moments of inertia, are used to quantify the shape of each bulk void. They are denoted as τ_1 , τ_2 and τ_3 such that $\tau_1 \leq \tau_2 \leq \tau_3$. In Figure ?? we show the computed distributions for τ_1/τ_2 and τ_2/τ_3 for voids larger than 8 cells in order to avoid statistic fluctuations due to small regions. We rather calculate histograms for these ratio quantities instead of each single value in order to avoid using an arbitrary normalization. For both schemes, it can be noticed that the shape distribution is completely spread out, thereby indicating a non-preferred geometry of void regions, which is in agreement with the well established high anisotropy of matter flows associated to this type of region.

For a better quantification, we also perform a classification of the shape of voids by setting a threshold in the analysed ratio quantities. An anisotropic or tri-axial shape correspond to voids where $\tau_1/\tau_2 < 0.7$ and $\tau_2/\tau_3 < 0.7$, where there is not any symmetry among the principal directions. We find about $57.2\% \sim 61.0\%$ of total voids consistent with this shape, for the T-web and V-web respectively. A pancake or quasi-oblate shape is associated to voids where $\tau_1/\tau_2 < 0.7$ and $\tau_2/\tau_3 > 0.7$. We found $13.1\% \sim 17.9\%$ of consistent voids. Filamentary or quasi-prolate voids satisfy $\tau_1/\tau_2 > 0.7$ and $\tau_2/\tau_3 < 0.7$, with $25.4\% \sim 18.1\%$ of all voids. Finally, isotropic or quasi-spheric voids are found when $\tau_1/\tau_2 > 0.7$ and $\tau_2/\tau_3 > 0.7$, with $4.2\% \sim 3.1\%$ of total voids compatible with this shape. The threshold value of 0.7 adopted here for the ratios of the moments of inertia is just for illustrative purposes, where such distinction is rather fuzzy and continuous. However, the previous analysis allows us to conclude that voids are quite asymmetric structures.

5.2 Density profile of voids

Describing the density profiles of voids is quite important in order to compare and match simulation with observational

surveys, allowing possible constrains for different cosmology models [Hamaous, et.al 2014]. Here, and taking into account the previous results, we rather use an ellipsoidal approximation to describe and fit the shape of bulk voids, so we use the next ellipsoidal radial coordinate to describe density profiles.

$$r^2 = \frac{x^2}{\tau_1^2} + \frac{y^2}{\tau_2^2} + \frac{z^2}{\tau_3^2}, \quad 0 \leq r \leq 1 \quad (6)$$

where we take the principal moments of inertia $\{\tau_i\}$ as the lengths of the principal axes of the ellipsoid and each one of the cartesian coordinates as measured in the rotated frame of each void.

We use the same analytic density profile that [Hamaous, et.al 2014] to fit the numerical density profiles of our voids.

$$\delta_v(r) = \delta_c \frac{1 - (r/r_s)^\alpha}{1 + (r/r_v)^\beta} \quad (7)$$

6 CONCLUSIONS

ACKNOWLEDGMENTS

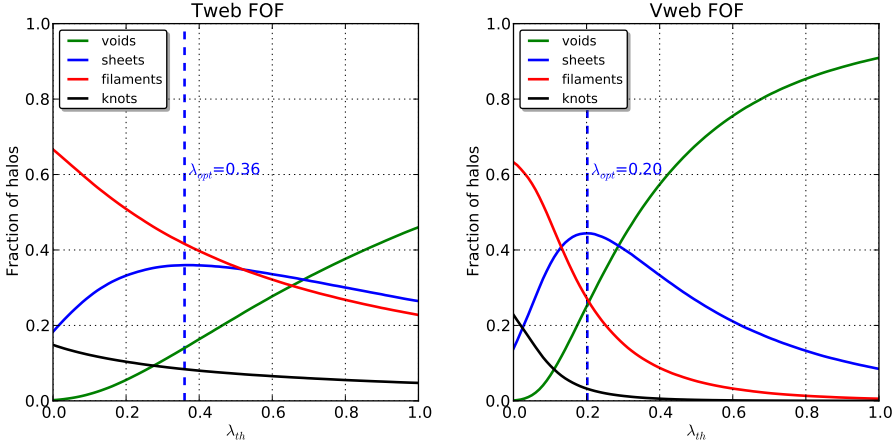


Figure 1. Fractions of halos embedded in each one of the defined environments according to the λ_{th} value. T-web scheme (left panel) and V-web scheme (right panel). The optimal parameters found are $\lambda_{opt}^T = 0.36$ and $\lambda_{opt}^V = 0.20$.

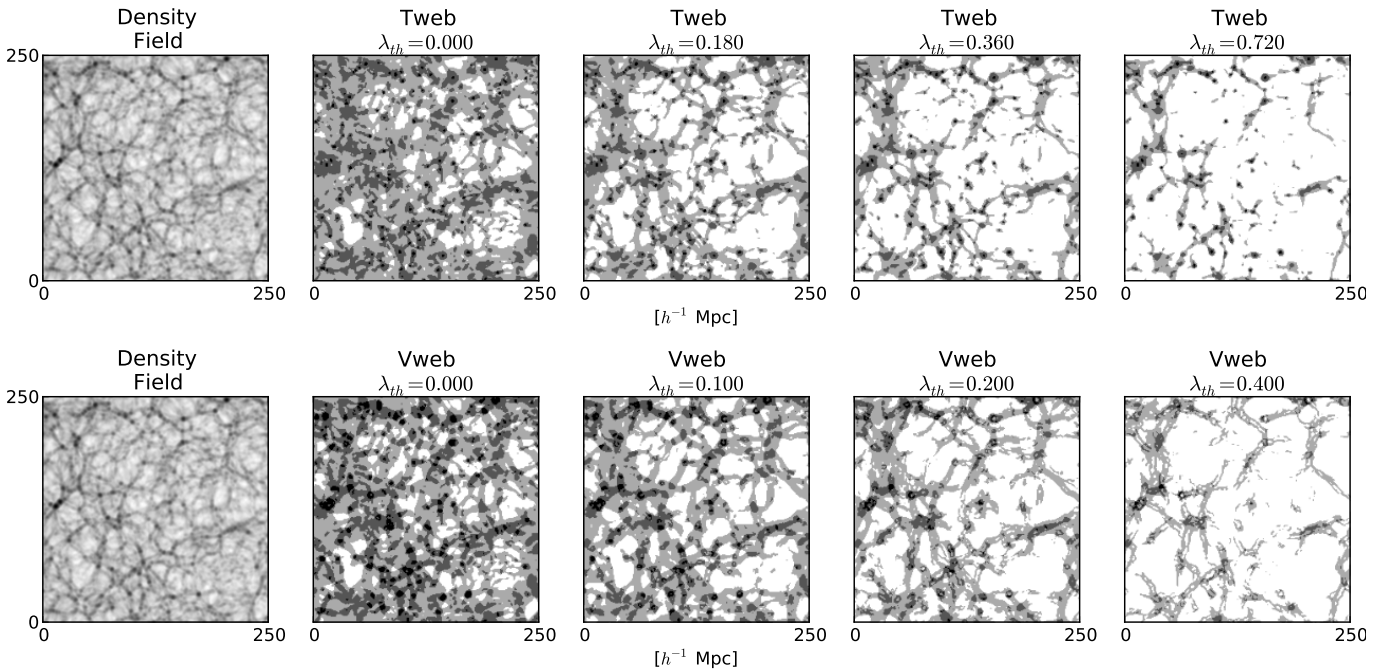


Figure 2. Visual impression of the density field (left panels), and of each classification scheme with the λ_{th} values obtained by our criteria (others panels). The color convention for each environment is (white) - void, (light gray) - sheet, (gray) - filament, (black) - knot. For each web scheme, it has been used the previously established optimal threshold as a reference value, so plots are done with the next values $\lambda_{th} = 0.0$, $\lambda_{th} = \lambda_{opt}/2$, $\lambda_{th} = \lambda_{opt}$ and $\lambda_{th} = 2\lambda_{opt}$.

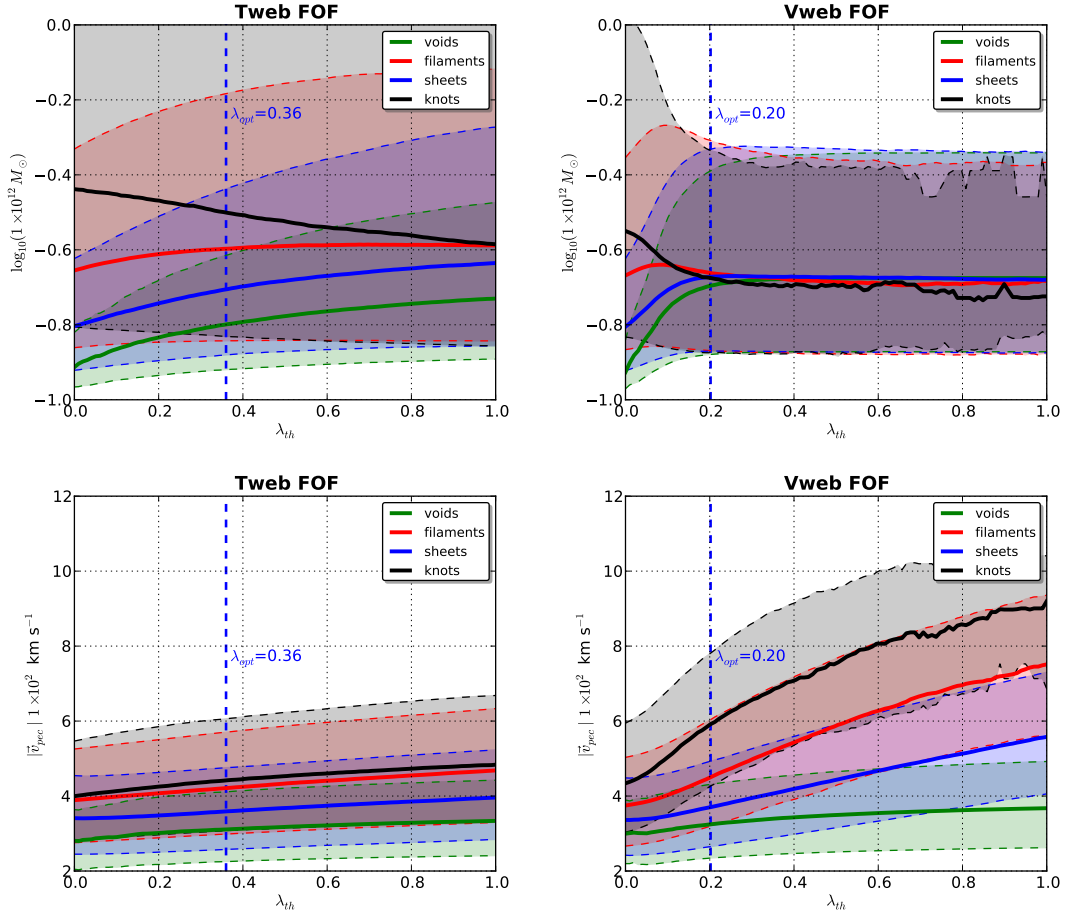


Figure 3. Distribution of masses of dark matter halos according the region where they are embedded for both web schemes (upper panels) and of peculiar velocity (lower panels). It can be noticed that the T-web scheme selects different mass ranges according to the environment, while the V-web scheme is better selecting ranges of peculiar velocity of the dark matter halos. This can be understood taking into account the physical origin of each web scheme.

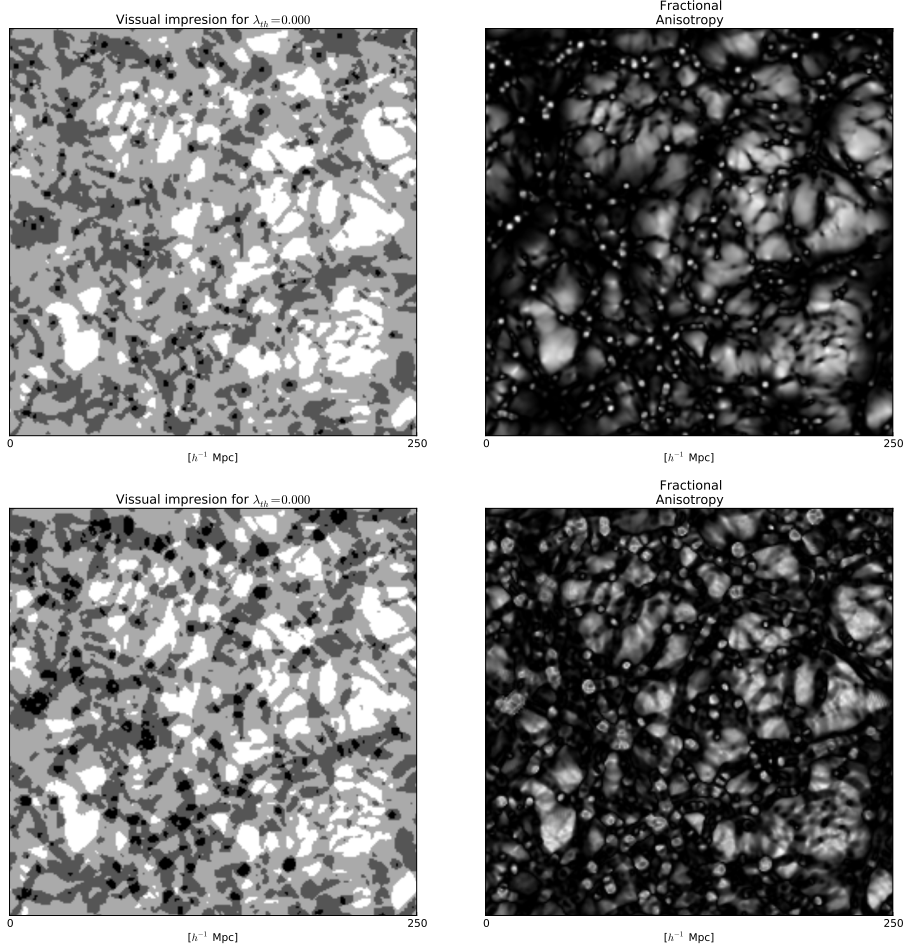


Figure 4. In left panels is shown the visual impression of the cosmic web for each web scheme (T-web, upper panels. V-web, lower panels) obtained for $\lambda_{th} = 0.0$. It can be seen each one of the defined types of environment, where voids corresponds to white zones, sheets to gray, filaments to dark gray and finally knots to black regions. In the right panels is shown the fractional anisotropy field for the same slide of the simulation and for each web schemes, where black regions correspond to $FA = 1$ and white regions to $FA = 0$. It can be noticed the degeneration of low values of FA for knots and central regions of voids, while high values of FA ($FA \lesssim 1$) are consistent with filaments and highly planar sheets.

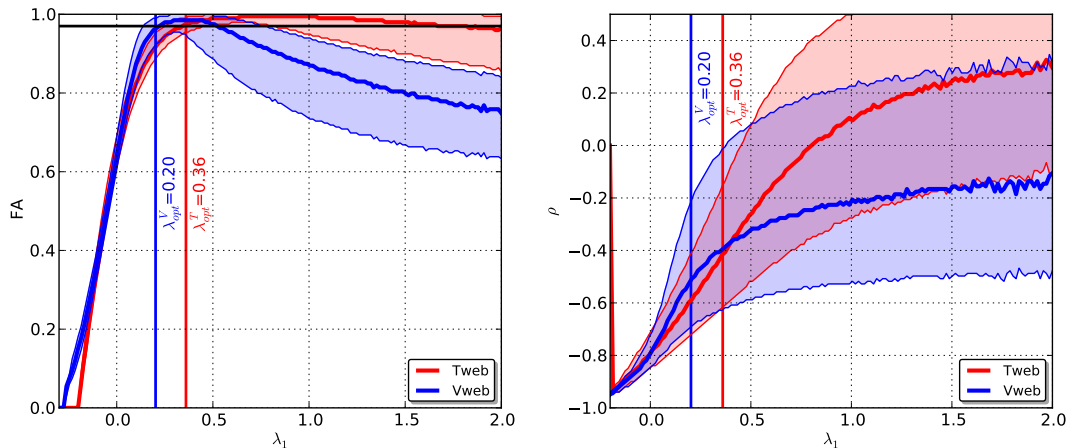


Figure 5. In this figure is shown the distribution of the fractional anisotropy (left panel) and density field (right panel) with respect to the eigenvalue λ_1 for each web scheme (T-web, red lines. V-web, blue lines) as calculated over all the cells of the grid. Thick central lines correspond to the median of the distribution and coloured regions to the 50% of the cells, delimited by quartiles Q_1 and Q_3 .

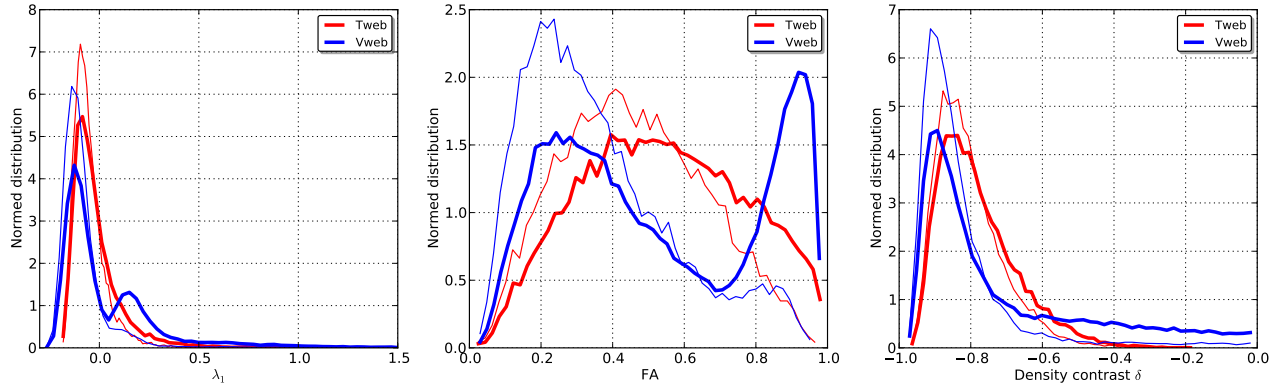


Figure 6. In this figure is shown the distribution of the fractional anisotropy (left panel) and density field (right panel) with respect to the eigenvalue λ_1 for each web scheme (T-web, red lines. V-web, blue lines) as calculated over all the cells of the grid. Thick central lines correspond to the median of the distribution and coloured regions to the 50% of the cells, delimited by quartiles Q_1 and Q_3 .